Comparative study of active infrared thermography, ultrasonic laser vibrometry and laser ultrasonics in application to the inspection of graphite/epoxy composite parts

V.P. Vavilov, A.A. Karabutov, A.O. Chulkov, D.A. Derusova, A.I. Moskovchenko, E.B. Cherepetskaya & E.A. Mironova

Published online: 31 Jul 2019.

Submit your article to this journal

View Crossmark data

Taylor & Francis
Taylor & Francis Group

Check for updates

Comparative study of active infrared thermography, ultrasonic laser vibrometry and laser ultrasonics in application to the inspection of graphite/epoxy composite parts

V.P. Vavilov[a], A.A. Karabutov[b,c,d], A.O. Chulkov[a], D.A. Derusova[a,e], A.I. Moskovchenko[a], E.B. Cherepetskaya[c] and E.A. Mironova[c]

[a]Thermal Testing Laboratory, Tomsk Polytechnic University, Tomsk, Russia; [b]Laser Center, ILC M.V. Lomonosov Moscow State University, Moscow, Russia; [c]Optoacoustics Laboratory, NUST MISIS, Moscow, Russia; [d]Laser Acoustics Laboratory, ILIT RAS – Branch of the FSRC «Crystallography and Photonics» RAS, Shatura, Russia; [e]Laboratory for quality control in materials and structures, Institute of Strength Physics and Materials Science, Siberian Branch, Russian Academy of Sciences, Tomsk, Russia

ABSTRACT

Three nondestructive testing techniques, namely, optically- and ultrasonically stimulated infrared thermography, ultrasonic laser vibrometry and laser ultrasonics, have been comparatively investigated in the inspection of a graphite-epoxy sample characterized by a complicated geometry to demonstrate advantages and drawbacks of each technique in the detection of different types of defects.

1. Introduction

Thermal nondestructive testing (TNDT) has proven to be a reliable technique for inspecting composite materials. Its undisputable advantages are a high productivity of testing and ability to detect defects that are characteristic for composites [1–3]. However, in one-sided test procedures, TNDT is limited by detection depth of about 4 mm (in graphite-epoxy composite) and difficulties in the analysis of material/defect microstructure conditioned by heat diffusion which 'smashes' defect indications. In some cases, these inspection drawbacks can be overcome by using special thermal characterization approaches based on advanced modelling and data processing [4,5]. Another solution is to utilize a screening character of TNDT by complementing inspection results with the data obtained by means of other techniques. Immersion ultrasonic nondestructive testing (NDT), in its classical form, is often mentioned in the conjunction with TNDT, also due to its ability to determine defect depth [6,7]. A novel-related technique is ultrasonic laser vibrometry allowing evaluation of surface vibrations in a scanning procedure with a high spatial resolution and documentation of results in an illustrative way [8–10]. As demonstrated in [10,11], the above-mentioned techniques may well complement each other in particular test cases allowing also data fusion.

Most previous studies in NDT of composite materials have been related to particular inspection techniques or particular types of defects in flat reference samples. In graphite-epoxy composites, either impact damage or insert-like defects have been investigated [12,13]. Few works were dedicated to the comparison of efficiency of various NDT methods applied to samples of complicated shape [10,14–19]. A technique of remote laser ultrasonic NDT seems to be useful in this case providing some new inspection opportunities [20–23]. Contact laser ultrasonic evaluation (CLUE) method [24,25] is close to conventional ultrasonic testing but provides significant enhancement of spatial resolution thus being suitable for analyzing material microstructure. This technique combines advantages of laser-excited ultrasonics and some dedicated data processing algorithms.

In this study, we apply three NDT techniques, namely, active infrared (IR) thermography (including both optical and ultrasonic stimulation), ultrasonic laser vibrometry and laser ultrasonics, to the detection of three types of defects (wall thinning, impact damage and cracks) in a curved part made of a graphite-epoxy composite. Such parts are widely used in the aviation and aerospace.

2. Test sample

A 250 × 100 × 2.5 mm graphite-epoxy test sample shown in Figure 1 represented a fragment of a composite cylindrical shell used in the aerospace (shell radius 0.5 m). This curved-shape sample was strengthened with two types of ribs also made of graphite epoxy and contained three artificial defects (specified as D1, D2 and D3 in Figure 1): 15 J impact damage, local wall thinning with 15 mm-diameter material loss from 40% to 50% and two 12 mm-long thin perpendicular slits simulating cracks and made by means of a 0.2 mm-thick blade. Since thinning-like ('corrosion-type') defects are not typical in real
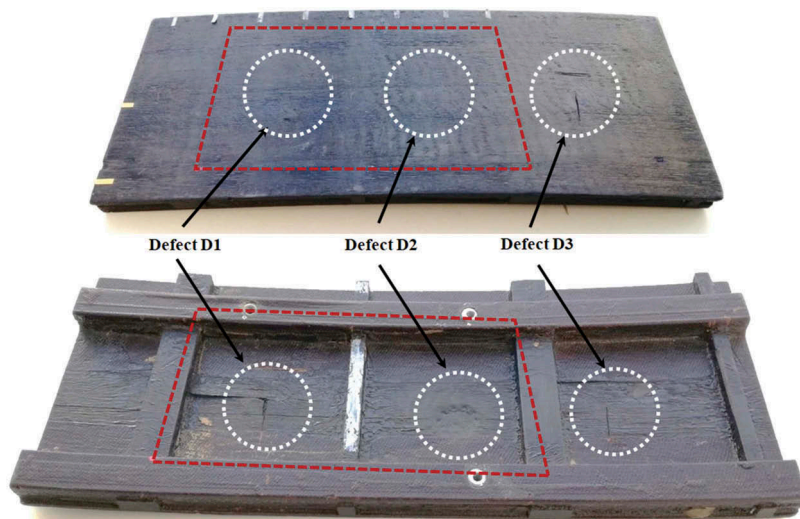

Figure 1. Graphite epoxy test sample (front, rear and cut views, D1 – 15 J impact damage, D2 – 40–50% wall thinning, D3 – two through-the-sample slits simulating 'kissing' cracks, red square dashed area was tested by laser ultrasonics).

composite parts, this kind of defects was used to show how local variations of main panel thickness and the presence of ribs affect surface temperature. Two other defects, in fact, simulated composite cracking that can occur in both lateral and in-depth directions. The through-the-sample cracks were scarcely detected visually, therefore, to some extent, they simulated vertical 'kissing' cracks which are typically hard to detect by applying conventional NDT techniques.

3. Inspection techniques and results

Five experimental setups implementing all inspection techniques used are shown in Figure 2.
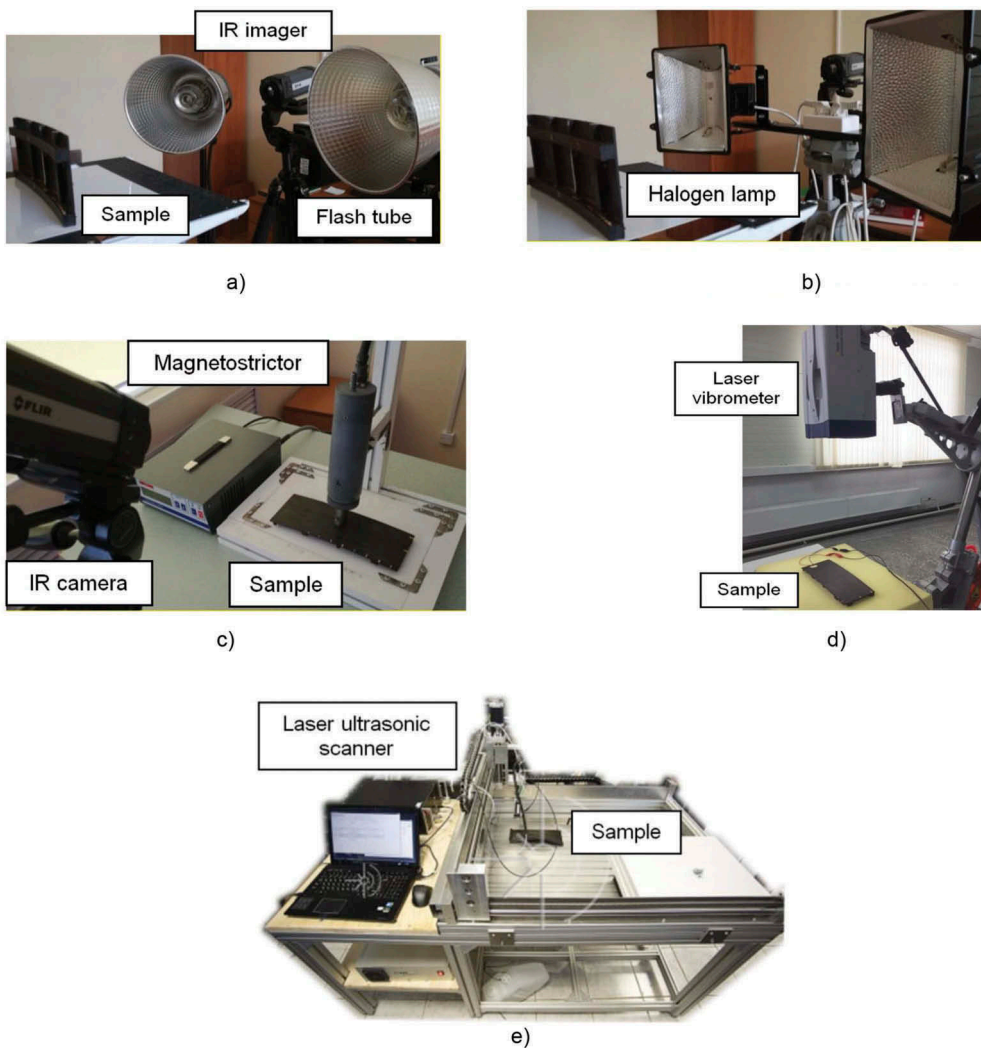

Figure 2. Experimental setups: (a)-optically-stimulated IR thermography (Xenon flash tubes), (b)- optically stimulated IR thermography (halogen lamps), (c)-ultrasonic IR thermography, (d)-ultrasonic laser vibrometry, € – laser ultrasonics.

3.1. Optically stimulated IR thermography

The active IR thermographic method has been applied in its 'classical' implementation, i.e. by involving optical and ultrasonic excitation. A flash tube (5 ms, 1600 J) and two halogen lamps (1 kW each) have been routinely used in a one-sided procedure to result in IR image sequences which included from 50 to 500 images recorded with the acquisition frequency of 10 Hz. Both pulsed and thermal wave test procedures have been implemented. The laboratory setup has been designed around a FLIR A325 (or Optris 450 as an alternative) IR module and included the home-made software providing data acquisition and processing by using the most of known TNDT algorithms, merely to mention Fourier and wavelet transforms, principle component analysis (PCA), thermographic signal reconstruction (TSR), correlation, normalization, etc [26]. An example of the raw image obtained by flash optical stimulation is shown in Figure 3(a). The performance of each NDT technique (except laser ultrasonics) has been evaluated by using the known concept of signal-to-noise ratio $SNR = |U_d - U_{nd}|/\sigma_{nd}$, where $U_{d,nd}$ are the signals in defect (D) and non-defect (ND) areas, and σ_{nd} is the signal standard deviation in a chosen non-defect area.

Flash heating was not powerful enough to ensure a detectable temperature elevation over the area with material loss while indications of two other defects clearly appeared in the raw image (Figure 3(a)); note that two 'cracks' (D3) are well resolved. Applying the technique of PCA has allowed to underline the material loss (SNR = 7) but worsened visibility of two other defects (Figure 3(b)). This is a typical selective feature of the PCA method which underlines particular types of temperature patterns in particular
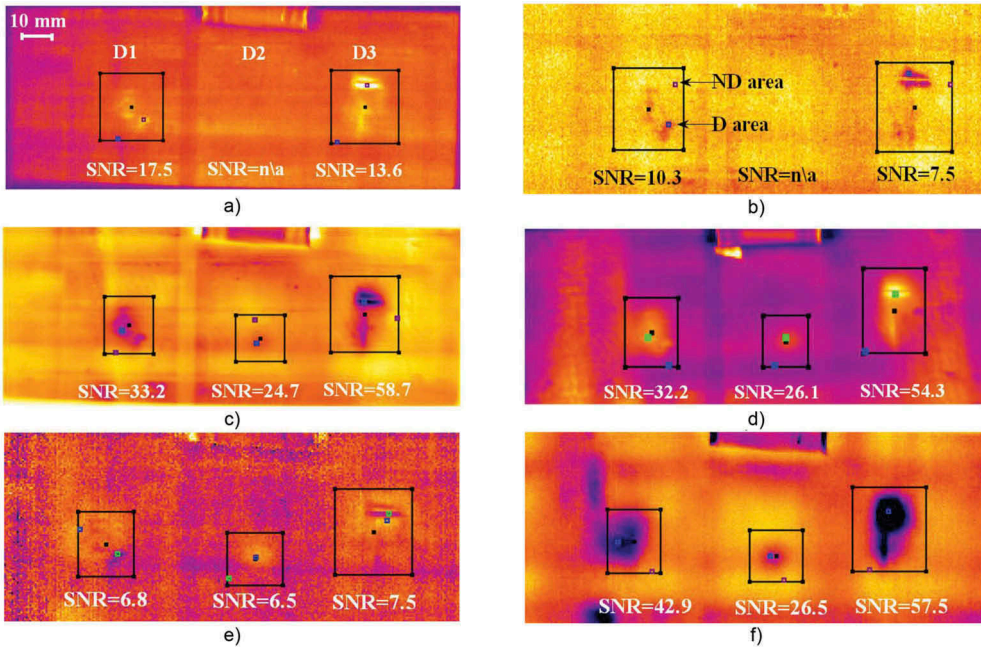

Figure 3. Test results, optical stimulation: (a)-Xenon tube heating, raw image, (b)-same as a), PCA image; (c)-halogen lamp heating for 10 s; PCA image; (d)-halogen lamp heating, thermal waves, frequency 0.03 Hz, Fourier ampligram, €- Xenon tube heating, TSR, first derivative; (f) – halogen lamp heating for 10 s, TSR, first derivative.

components. The thermogram in Figure 3(c) illustrates why halogen lamps are often used in active TNDT devices due to high energy delivered for some seconds of heating (see the results of the pulsed test in Figure 3(c)), even if the defect patterns look blurred because of lateral heat diffusion. The highest SNR values for the defects D1 and D3 appeared in the case of low-frequency (0.03 Hz) thermal waves(Figure 3(d)), while the defect D2 was reliably detected after having applied the TSR technique in the halogen lamp heating procedure (Figure 3(f)).

3.2. Ultrasonically stimulated IR thermography

Ultrasonic stimulation was performed by using a magnetostrictive device which provided continuous (long-pulse) stimulation with 22 kHz mechanical waves, while the electric power supplied to the magnetostrictive indentor was in the range from 50 to 500 W (see also [13,15]). When the indentor was firmly pressed onto the sample front surface in the sample bottom centre, the defects D1 and D3 have been reliably detected providing very high SNR values (Figure 4). In fact, the temperature signals in defect areas were linearly proportional to the electric power, even if an effective power of ultrasonic waves introduced into material was quite low. By shifting the indentor closer to one of the two defects (D1 or D3), one may improve the visibility of this defect but worsens the signal in the area of another defect. In fact, the central position of the indentor provided the best simultaneous visibility of the defects D1 and D3 while the defect D2 (wall thinning) can hardly be detected by ultrasonic IR thermography because of a lack of internal friction. High SNR values which are typical for this NDT technique are conditioned by the principle of 'dark field' that is characteristic for ultrasonic IR thermography. This means that defect-free areas do not change their temperature as a result of stimulation thus leading to low values of the temperature standard deviation σ_{nd}. The noticeable divergence in the SNR values in Figure 4 is explained by a strong non-linear dependence of the temperature signals on the position of a stimulation point while moving the indentor across the sample.

3.3. Ultrasonic laser vibrometry

The technique of laser vibrometry combined low-power ultrasonic stimulation and vibration measurement by using a scanning laser Doppler vibrometer PSV-500-3D
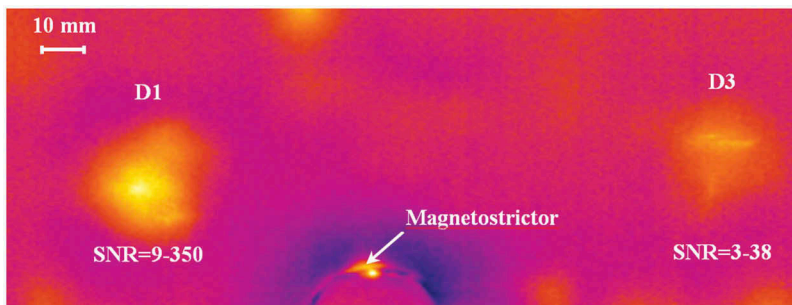

Figure 4. PCA image (second component) of sample surface under ultrasonic stimulation (22 kHz, 300 W electric power).

from Polytec (see also [8,11–15]). The input voltage with the amplitude of up to 120 V was supplied from an AWG-4163 generator via a voltage amplifier AVA-1810 to the piezoelectric transducer FT-27T clamped onto the front side of the sample. This allowed exciting flexural waves in the frequency band from 25 Hz to 100 kHz with the accuracy of ±25 Hz. A scanned area consisted of 50 × 50 points that was equivalent to a 3 mm scan step. The total vibration pattern clearly showed the defects under a relatively low ultrasonic load (~50 mW of acoustic power), see Figure 5. The mean magnitude of vibration velocities over defects varied from 0.7 to 1.5 mm/s while the amplitude of vibration velocity in defect-free areas was about 0.2 mm/s. In this way, the difference in velocities resulted in the values of signal-to-noise ratio of 11, 5 and 12 for the defects D1, D2 and D3, respectively. It is worth noting that, when performing laser vibrometry, the inspection time reached 4 min if resonance frequencies adherent to the defects were not preliminarily found. But the need for determining particular resonances approximately doubled this time. The presence of ribs in the sample essentially diminished the intensity of surface vibrations resulting in the areas of lower vibration amplitudes undetected in Figure 5.

The most important information about defects is supplied by analyzing amplitude-frequency characteristics of samples under test. For each of three defects, both the proper frequency ranges and the resonance frequencies with maximal local vibrations were found (Figure 6). Since the resonance vibrations in the defect areas were observed at frequencies from 2 to 3.6 kHz, only the section of the total amplitude frequency characteristic from 1 to 10 kHz was investigated in details (Figure 7). For each of three resonance frequency bands, a Q-factor was determined as a parameter which describes how underdamped is an oscillator (Table 1). A Q-factor also shows its bandwidth in relation to the centre frequency f_{LDR}. It follows from Table 1 that the lowest energy loss determined in regard to the stored energy of the resonator corresponds to the defect D2 (Q = 38). At the frequency of 2.28 kHz, the D3 area was characterized by the mean vibration velocity of the local defect resonance (V_{LDR}) equal to 62 µm/s and produced SNR = 23 in regard to the mean 'non-defect' vibration velocity ($V_{outside}$) of 4.05 µm/s (see the formula for SNR above). In the D2 area, the intensity of resonance vibrations exceeded those in a non-defect area by 14 times reaching the value of 51 µm/s at the frequency of 3.25 kHz; the corresponding SNR value was 21. Respectively, in the D1 area, the mean vibration amplitude was 73 µm/s at the frequency of 2.65 kHz (mean 'non-defect' value was 6.5 µm/s) with the maximum SNR = 22. It is important noting that, in
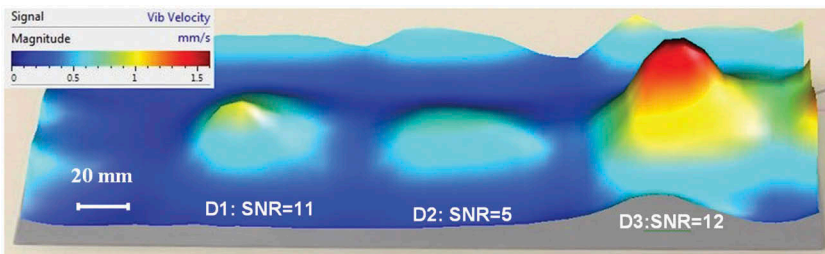

Figure 5. Total vibration pattern obtained under low-power ultrasonic stimulation by applying SLDV technique (25 Hz – 100 kHz frequency range).
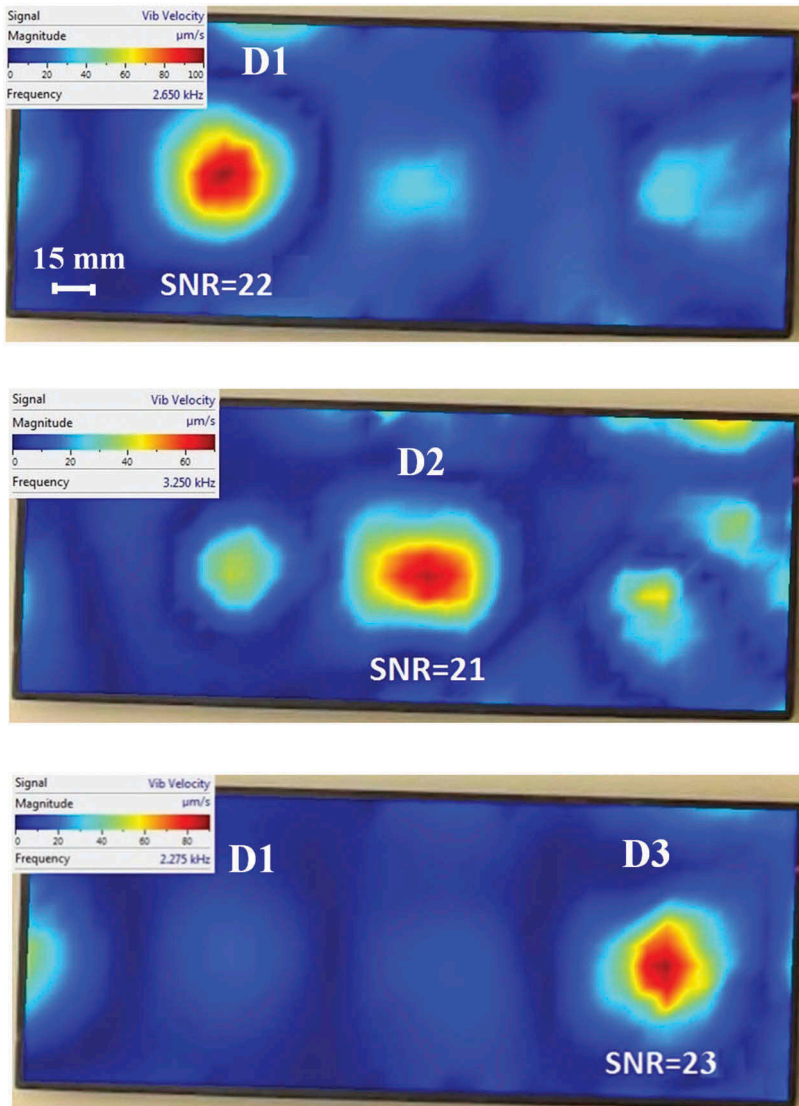
Figure 6. Local resonance vibrations: D1 – 2.65 kHz (top), D2 – 3.25 kHz (middle), D3 – 2.28 kHz (bottom).

spite of essentially different Q-values for three defects, the corresponding SNR values are close thus confirming a high quality of the local resonances.

Since the resonance frequencies for all defect areas were close, the technique of laser vibrometry allowed obtaining clear defect patterns in the image of total vibrations even if the corresponding SNR values were 2–4 times lower than in the case of resonance stimulation (Figure 5, 25 Hz–100 kHz frequency range).

It is believed that the technique of resonance ultrasonic IR thermography allows the determination of defect location and dimensions by total vibration patterns for some minutes with a reasonable spatial resolution (few mm). However, a test time may
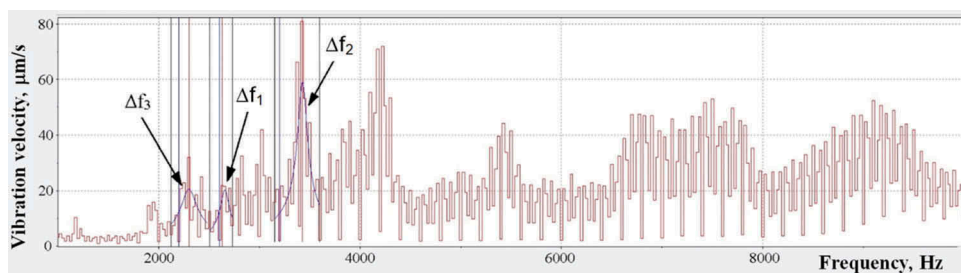
Figure 7. Amplitude-frequency characteristics of sample surface vibrations in the frequency range from 1000 Hz to 10,000 Hz (resonance frequencies Δf_1, Δf_2 and Δf_3 are shown for the defects D1, D2 and D3).

Table 1. Apparent defect areas and damping characteristics of defects in graphite-epoxy sample.

Defect	f_{LDR}, Hz	Δf, kHz	$V_{LDR}/V_{outside}$	Q-factor	Defect area, mm^2	SNR
D1	2.65	2.5–2.73	11.2	31	1485	23
D2	3.25	3.15–3.6	14	38	1980	21
D3	2.28	2.13–2.5	15	15	1810	22

become too long if, while determining local resonances, the number of spectral lines should be high enough to allow the efficient Fourier transform, and/or the number of scanned points should be increased. In this case, SNR values can be enhanced by 2–4 times (in a particular experiment) but the test time will be twice longer. In fact, a needed test time can be chosen by the operator depending on inspection task and a required efficiency of defect evaluation.

3.4. Laser ultrasonics

Laser ultrasonics utilizes broad-band ultrasonic waves generated by a laser pulse. The waves scattered by structural inhomogeneities of composites can be analyzed with a high temporal resolution thus allowing depth evaluation more efficiently that in the case of conventional ultrasonic NDT. The probe pulse width is 70 ns to provide the frequency band from 0.2 to 6.6 MHz at half maximum and the in-depth resolution of about 0.2 mm in metals like steel and aluminium. The 65 dB dynamic range allows investigation of materials with high ultrasonic attenuation, such as composites.

The size of the scanned area was 150 × 80 mm (see Figure 1), the ultrasonic beam diameter – 3.4 mm, and the scanning step – 2 mm. The pulse repetition rate of 1 kHz enabled the measurement of 10–20 points per second. The signals obtained can be represented in XY, XZ and YZ planes which depict the sample cross-sections (slices) at particular coordinates Z, Y and X, respectively. The corresponding examples are shown in Figure 8 for the defects D1 and D2 (the sample area with the defect D3 was not scanned). The X and Y coordinates are identified by position of both the vertical and horizontal markers on the XY-plane, and, correspondingly, the Z-coordinate is determined by the horizontal marker on the XZ plane. By changing the position of markers, it is possible to visualize the internal structure of the sample, as shown in Figure 8. The damage of the composite is evidently seen. The dark areas
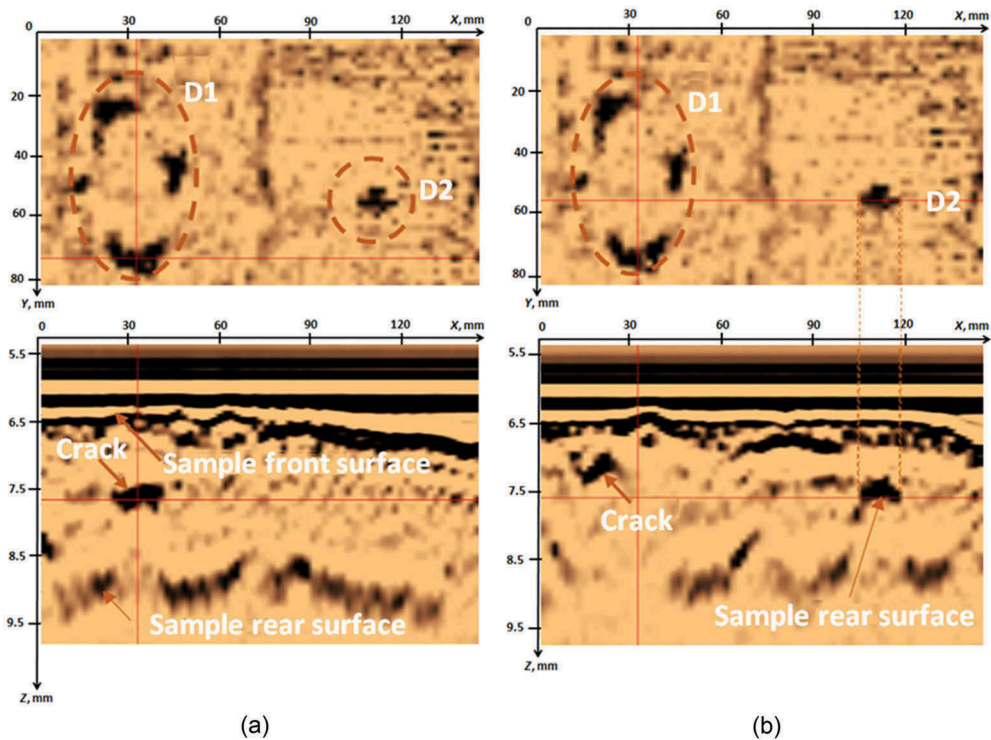
Figure 8. Example of laser ultrasonic test results: (a) XY, XZ-planes in the area of defect D1, (b) XY, XZ-planes in the area of defect D2.

show both impact-induced delaminations (D1) and material loss (D2). The Z-coordinate corresponds to the time delay of the acoustic signal. In fact, by knowing velocity of ultrasonic waves in a test material, one can convert time delays in the in-depth coordinate Z (note that the dark areas in Figure 8 reflect signal amplitudes). In many cases, the presence of a distinct bottom signal allows self-calibration of results by defect depth. For example, the D2 defect is located at the depth of 1.3 mm and its effective reflection spot is characterized by the diameter of 13 mm thus corresponding to the true size of this defect.

In Figure 9, the sample front surface is represented by a light-colour top line because here ultrasonic pulses penetrate the composite from the medium of a lower density. Respectively, the rear surface appears as a wide dark line. The main feature of the images in Figure 9 is that the composite is essentially inhomogeneous. The area of impact damage (D1) contains plentiful cracks propagating along fibre directions while the rear-surface signals are absent. This is explained by the fact that acoustic signals cannot penetrate through the area of damage.

Thanks to a high spatial resolution of laser ultrasonics, the results of applying this test method are sensitive to small variations in composite density thus producing images of which treatment is not straightforward but requires a considerable operator's experience. A figure of merit for laser ultrasonic images is the local variation of acoustic impedance that is the product of the ultrasonic wave velocity and density. Therefore,
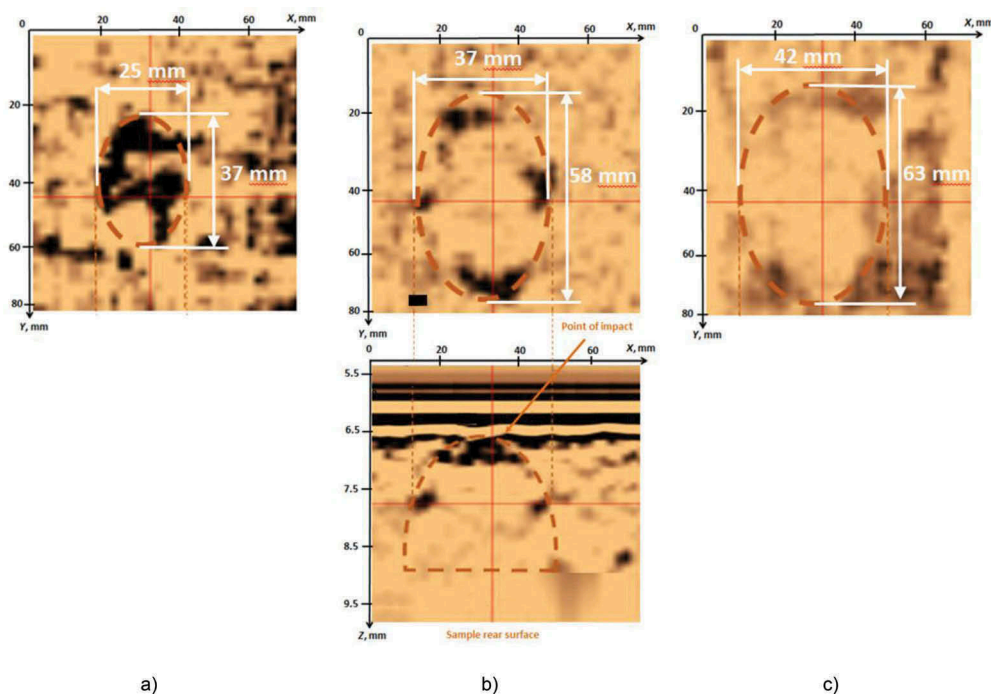
Figure 9. XY (top row) and XZ (bottom row) slices in the area of D1: (a) - depth 0.5 mm, (b) - 1.3 mm, (c) – 2.7 mm.
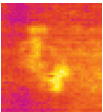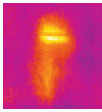
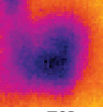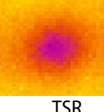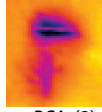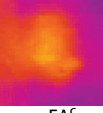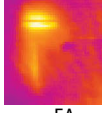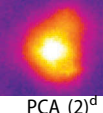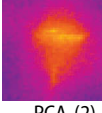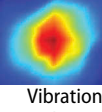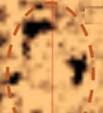the areas with delaminations, disbonds, excessive porosity, etc., look 'darker' in regard to areas of a regular texture. On the other hand, if the object texture is 'rough', the contrast of defects can be relatively low. For example, fibre waviness results in images of a lower contrast because, in the presented case, the slice thickness is about 15 μm, and the defects partially occupy other slices.

Figure 9 shows some sets of slices in the area of the defect D1. The XY-planes correspond to different material depths, approximately 0.5, 1.3 and 2.7 mm, while the in-depth propagation of the damage is illustrated by the XZ-slice along the horizontal lines. Considering these results, one can see that the zone of internal structure damage has the form of an inverted cup with the cup bottom corresponding to the surface point of impact. The cracks shown in the XY-slices look like concentric ellipses of which size increase with depth (ellipse axes ratio was about 1.5).

3.5. Table of results

Summarized results of applying all NDT techniques are presented in Table 2. Both SNR and maximal/minimal apparent defect lateral dimensions were used for comparison. Values of SNR were determined by using an automated algorithm based on searching for maximal and minimal signal amplitudes in a chosen area thus significantly reducing operator's involvement [27]. The highest SNR values were provided by ultrasonic IR thermography due to the above-mentioned principle of the 'dark field'. In the case of

Table 2. Summarized test results.

Type of stimulation	D1 (impact damage)			D2 (wall thinning)			D3 (two through-the-sample cracks)		
	Image	SNR	Apparent lateral size, mm	Image	SNR	Apparent lateral size, mm	Image	SNR	Apparent lateral size, mm
Optical pulsed (Xenon tube)	RI[a]	18	18 × 28	-[b]	-	-	PCA (1)	8	37 × 19
Optical pulsed (halogen lamps)	TSR	43	19 × 23	TSR	27	10 × 12	PCA (2)	59	32 × 17
Optical thermal wave (halogen lamps)	FA[c]	32	18 × 14	FA	26	9 × 8	FA	54	23 × 11
Ultrasonic IR thermography	PCA (2)[d]	350	43 × 28	-	-	-	PCA (2)	38	33 × 21
Ultrasonic laser vibrometry	Vibration velocity	23	48 × 48[e]	Vibration velocity	21	57 × 48[d]	Vibration velocity	22	45 × 42[e]
Laser ultra-sonics[f]		-	63 × 42		-	13 × 11		-	-

[a]Raw image.
[b]Data non-available.
[c]Fourier ampligram.
[d]PCA component image.
[e]Defect area differs from that in Table 1 because of the non-square shape of the defect.
[f]Laser ultrasonics results need further exploration.

optical stimulation, high SNR values appeared after data processing by using the TSR method.

Apparent defect lateral dimensions were evaluated by the operator using a known image scale, and this process was characterized by certain arbitrariness, although, first of all, the results depended on a physical nature of signals. Thus, all techniques of optical stimulation produced close estimates of defect size, while the techniques of ultrasonic IR thermography and laser vibrometry showed larger defect areas where mechanical vibrations took place. The inspection by means of laser ultrasonics represented a special case where the estimates of defect area depended on slice depth and, to some extent,

operator's experience. In general, the issue of determining defect size by different physical NDT methods requires further analysis.

4. Conclusion

'Classical' IR thermographic NDT based on optical stimulation remains a reliable technique in the detection of various types of defects in graphite-epoxy composites, in particular, if defects are laterally extended. Impact damage in composites can be effectively evaluated if cracking is fairly shallow. Deeper structural imperfections can be detected in a two-sided procedure or in a one-sided procedure applied to a rear surface of the sample. Active thermal NDT can be effectively complemented with ultrasonic stimulation which might be preferable if 'kissing' defects are to be detected. In this case, test results are weakly dependent on defect depth. Ultrasonic laser vibrometry combined with the principle of ultrasonic resonance stimulation appears as a very sensitive NDT method but it is still time-consuming and expensive. Both techniques involving ultrasonic stimulation have demonstrated apparent defect size larger than in the case of optical stimulation. The technique of laser ultrasonics seems to be a good addition to other NDT techniques due to its very high spatial resolution and tomographic data presentation. But this technique is also time-consuming and requires high operator's qualification when identifying composite structural inhomogeneities. However, it enables the most detailed analysis of distribution and size of structural defects in materials. The future research will be devoted to developing methodology of data fusion by using NDT techniques based on various physical principles.

Disclosure statement

No potential conflict of interest was reported by the authors.

Notes on contributors

V.P. Vavilov is a professor at Tomsk Polytechnic University. His area of expertise covers thermal testing, heat conduction and image processing.

A.A. Karabutov is a professor at Moscow State University specializing in laser acoustics.

A.O. Chulkov is a senior researcher at Tomsk Polytechnic University. His research area is development of thermal NDT equipment and experimentation.

D.A. Derusova is a senior researcher at Tomsk Polytechnic University. Her research area is related to laser vibrometry and NDT.

A.I. Moskovchenko is a PhD student at Tomsk Polytechnic University focused on general aspects of thermal NDT in the aerospace industry.

E.B. Cherepetskaya is a senior researcher at NUST MISIS. Her research area covers laser acoustics and ultrasonic NDT.

E.A. Mironova is a professor at NUST MISIS specialized on laser acoustics and applications to NDT of composites.

References

[1] Sfarra S, Fernandes HC, López F, et al. Qualitative assessments via infrared vision of subsurface defects present beneath decorative surface coatings. Int J Thermophys. 2018;39 (1).
[2] Lei L, Bortolin A, Bison P, et al. Detection of insulation flaws and thermal bridges in insulated truck box panels. Quant Infrared Thermogr J. 2017;14(2):275–284.
[3] Dong B, Pan B, Zhang Y, et al. Microdefect identification in polymers by mapping depth-resolved phase-difference distributions using optical coherence tomography. Polym Test. 2018;68:233–237.
[4] Altenburg SJ, Weber H, Krankenhagen R. Thickness determination of semitransparent solids using flash thermography and an analytical model. Quant Infrared Thermogr J. 2018;15 (1):95–105.
[5] Guo X, Zhang N. A phase sensitive modulated thermography of debondings in the insulator of SRMs. Polym Test. 2017;57:226–234.
[6] Soldatov AA, Soldatov PV, Soldatov AI, et al. Small-angle acoustic tomography under shadow testing with antenna arrays. Russ J Nondestr Test. 2018;54(7):463–468.
[7] Wang Y, Hu HX, Liu SJ, et al. The effect of water-cement ratio on acousto-ultrasonic characteristics in mortar. Russ J Nondestr Test. 2017;53(2):148–158.
[8] Solodov I, Dillenz A, Kreutzbruck M. A new mode of acoustic NDT via resonant air-coupled emission. J Appl Phys. 2017;121(24):245101.
[9] Hettler J, Tabatabaeipour M, Delrue S, et al. Detection and characterization of local defect resonances arising from delaminations and flat bottom holes. J Nondestr Eval. 2017;36(2).
[10] Balageas D, Maldague X, Burleigh D, et al. Thermal (IR) and other NDT techniques for improved material inspection. J Nondestr Eval. 2016;35(18):1–18.
[11] Post W, Kersemans M, Solodov I, et al. Non-destructive monitoring of delamination healing of a CFRP composite with a thermoplastic ionomer interlayer. Compos Part A Appl Sci Manuf. 2017;101:243–253.
[12] Klepka A, Pieczonka L, Staszewski WJ, et al. Impact damage detection in laminated composites by non-linear vibro-acoustic wave modulations. Compos Part B Eng. 2017;65:99–108.
[13] Vavilov V, Chulkov A, Derusova D. IR thermographic characterization low energy impact damage in carbon/carbon composite by applying optical and ultrasonic stimulation. Proc SPIE. 2014;9105:1–9.

[14] Rizi AS, Hedayatrasa S, Maldague X, et al. FEM modeling of ultrasonic vibrothermography of a damaged plate and qualitative study of heating mechanisms. Infrared Phys Technol. 2013;61:101–110.

[15] Solodov I, Bai J, Bekgulyan S, et al. A local defect resonance to enhance acoustic wave-defect interaction in ultrasonic nondestructive testing. Appl Phys Lett. 2011;99 (211911):109.

[16] Yang R, He Y. Optically and non-optically excited thermography for composites: a review. Infrared Phys Technol. 2016;76:26–50.

[17] Castanedo CI, Genest M, Guibert S, et al. Inspection of aerospace materials by pulsed thermography, lock-in thermography and vibrothermography: a comparative study. Proc SPIE. 2007;6541:1–9.

[18] He Y, Yang R. Eddy current volume heating thermography and phase analysis for imaging characterization of interface delamination in CFRP. IEEE Trans Ind Inform. 2015;11(6):1287–1297.

[19] Abdulrahman YA, Omar MA, Said ZA. Taguchi design of experiment approach to pulse and lock in thermography, applied to CFRP composites. Compos Nondestr Eval. 2017;72(36):1–11.

[20] Scruby CB, Drain LE. Laser ultrasonics: techniques and applications. Bristol (UK): Adam Hilger; 1990.

[21] Monchalin JP. Progress towards the application of laser-ultrasonics in industry. Rev Prog Quant Nondestr Eval. 1993;12a:495–506.

[22] Monchalin JP. Laser-ultrasonics: from the laboratory to industry. Review of progress in quantitative nondestructive evaluation. AIP Conf Pros. 2004;700:3–31.

[23] Pelivanov I, Buma T, Xia J, et al. A new fiber-optic non-contact compact laser-ultrasound scanner for fast non-destructive testing and evaluation of aircraft composites. J Appl Phys. 2014;115(113105).

[24] Podymova NB, Karabutov AA, Belyaev IO. Broadband laser-ultrasonic spectroscopy for quantitative evaluation of porosity effect on acoustic attenuation and phase velocity in CFRP composites. Proc 11th Europ. Conf. NDT (ECNDT 2014), 2014 Oct 6-10, Prague; Czech Republic; 2014. p. 10.

[25] Karabutov AA, Podymova NB. Broadband laser-ultrasonic spectroscopy for quantitative characterization of porosity effect on acoustic attenuation and phase velocity in CFRP laminates. J Nondestr Eval. 2014;33(1):141–151.

[26] Vavilov VP, Burleigh DD. Review of pulsed thermal NDT: physical principles, theory and data processing. NDT E Int. 2015;73:28–52.

[27] Chulkov AO, Vavilov VP, Nesteruk DA. An automated practical flaw-identification algorithm for active thermal testing procedures. Russ J Nondestr Test. 2018;54(4):278–282.